Resonant charge exchange and the transport of ions at high electric-field to gas-density ratios (E/N) in argon, neon, and helium

M. V. V. S. Rao,* R. J. Van Brunt,† and J. K. Olthoff
National Institute of Standards and Technology, Gaithersburg, Maryland 20899
(Received 8 April 1996)

Translational kinetic-energy distributions of singly and doubly charged ions have been measured at high electric-field to gas-density ratios (E/N) up to 5.0×10^{-17} V m^2 (50 kTd) in diffuse, parallel-plate Townsend discharges in Ar, Ne, and He using an ion energy analyzer-mass spectrometer. For Ar^+ in Ar and Ne^+ in Ne when $E/N<2.0\times10^{-17}$ V m^2 and for He^+ in He when $E/N<1.0\times10^{-17}$ V m^2, the energy distributions are Maxwellian and consistent with predictions based on the assumption that resonant symmetric charge exchange is the dominant ion–neutral-species collision process. At higher E/N values, the kinetic-energy distributions for Ar^+, Ne^+, and He^+ show departures from the Maxwellian form that are indicative of deviations from the charge-transfer model. The mean ion energies (effective ion temperatures) are consistent in the low E/N range with the available drift-velocity data, and in the case of Ar^+ with recent results of Radovanov *et al.* [Phys. Rev. E **51**, 6036 (1995)] from Townsend discharge experiments. The charge-exchange cross sections derived from Maxwellian fits to the energy distribution data for Ar^+ + Ar, Ne^+ + Ne, and He^+ + He agree with available data. The relative contributions of the doubly charged ions Ar^{2+}, Ne^{2+}, and He^{2+} to the total ion flux were found to be small (less than 3%) and tend to decrease initially with increasing E/N. The mean energies of the doubly charged ions are higher than those for the corresponding singly charged ions, and the results suggest that double charge transfer could be the dominant process affecting the transport of Ar^{2+} and Ne^{2+} for E/N below about 1.5×10^{-17} V m^2. The observed He^{2+} kinetic-energy distributions are not consistent with a charge-transfer model. [S1063-651X(96)10711-X]

PACS number(s): 52.80.Dy, 34.70.+e, 82.30.Fi, 51.50.+v

I. INTRODUCTION

Resonant symmetric charge exchange is presumed to be the predominant type of ion-atom collision that determines the kinetic-energy distributions of singly charged positive ions in the cathode fall region or sheath of low-pressure glow discharges in rare gases [1–9]. Recent experimental work of Radovanov and co-workers [10] has shown that the kinetic-energy distributions of Ar^+ in a diffuse Townsend discharge are Maxwellian and consistent with predictions of a simple charge-transfer model derived by Wannier [11] (also see [9] and [12]) for electric-field to gas-density ratios (E/N) up to about 2×10^{-17} V m^2 (20 kTd, 1 Td $\equiv10^{-21}$ V m^2). However, there are indications from this work that at $E/N=2\times10^{-17}$ V m^2, the charge-transfer model begins to fail. Mase and co-workers [13] have clearly shown from low-pressure drift-tube experiments that at sufficiently high effective E/N, the kinetic-energy distribution of Ar^+ in Ar will exhibit significant deviations from Maxwellian behavior with a high-energy tail or peak indicative of "runaway" or "beamlike" ions that experience few if any collisions in traversing the drift tube. It should be noted that departures from Maxwellian behavior have also been seen for He^+ in He, Ne^+ in Ne, and Ar^+ in Ar from the measured ion-velocity distributions of Ong and Hogan [14] for relatively low E/N, below 3.2×10^{-19} V m^2 (320 Td). At low E/N, the measured ion-energy distributions are susceptible to distortions arising from low-energy ion discrimination, ion absorption, and ion-surface interactions at the metal sampling plate [15,16].

Very little experimental data exist on the kinetic-energy distributions of positive ions in rare gases at high E/N (above 1×10^{-18} V m^2). In order to obtain data at E/N above the breakdown strength of the gas where drift tubes fail, it has been necessary to resort to the use of low-density, diffuse parallel-plate discharges generally known as Townsend discharges. A Townsend discharge corresponds to conditions immediately above breakdown inception near the Paschen minimum where the voltage drop across the electrodes is nearly independent of the discharge current [17–19]. In this type of discharge, the charged-particle densities are too low to significantly perturb the electric-field strength between parallel electrodes, and therefore, assuming a uniform gas density, the discharge region can be characterized as having a constant and uniform E/N. The positive ions are initially produced throughout the discharge volume by electron impact, and because of the nature of electron multiplication in the discharge, the ion density is expected to be nonuniform and peaked near the anode.

In an earlier work, Hornbeck [20] used a pulsed Townsend discharge to measure the drift velocities of ions in helium, neon, and argon for E/N up to about 2×10^{-18} V m^2. The measurements mentioned above by Radovanov and co-workers [10] of ion kinetic energies in argon at high E/N were performed using self-sustained Townsend discharges, as were the measurements in the present work. Although the experimental approach is similar to that taken in our earlier work [10], the apparatus used here, including the

*Permanent address: Institute for Plasma Research, Bhat, Gandhinagar, 382 424 India.
†Electronic address: vanbrunt@EEEL.nist.gov

S_i' merely represents a linear extrapolation of the low-energy portion of the distribution for $\varepsilon < 5.0$ eV in the calculations of $\langle \varepsilon \rangle$ and R.

IV. RESULTS

A. Kinetic-energy distributions

Examples of measured ion-kinetic-energy distributions (S_i versus ε_i) are presented in Figs. 4, 5, and 6, respectively, for Ar^+, Ne^+, and He^+. Shown in each case are the distributions at three widely separated values of E/N together with fits using the form of Eq. (5) (dashed lines) and Eq. (6) (solid lines). The intensities S_i correspond to the total number of counts/s that were recorded at each energy, i.e., the distributions, as shown, have not been normalized. As seen from the data for $\varepsilon_i > 60$ eV in the top graph of Fig. 6, the contribution of noise counts to the recorded signals is typically much less than 1% over the observed energy ranges. All of the data displayed in Figs. 4–6 were obtained for a gap spacing of 2.0 cm. No data points are shown for energies below 5.0 eV, where effects due to the finite energy resolution are known to distort the energy distribution. In some cases, energy discrimination effects appeared to extend somewhat above 5.0 eV as evident by the appearance of maxima in the distributions. The distorting effects noted by Skullerud and Holmstrom [15] due to ion-electrode interactions, most evident at E/N below about 1×10^{-19} V m^2, are not expected to be important here for energies above 5 eV.

It is seen that, in all cases, the difference between the two fits to the data are barely noticable, especially at the lower values of E/N. In general, if a good fit to the data is obtained using the model based on Eq. (5), then an equally good fit is obtained using the Maxwellian approximation given by Eq. (6). This implies, as indicated in Tables I–III, that β is small and the assumption of constant charge-transfer cross sections for $Ar^+ + Ar$, $Ne^+ + Ne$, and $He^+ + He$ is reasonable. It should be noted that, in fitting the forms of Eqs. (5) and (6) to the data, maxima that appeared in S_i versus ε_i for $\varepsilon_i > 5.0$ eV were ignored.

Above about 2×10^{-17} V m^2 (20 kTd) for argon and neon and above about 1×10^{-17} V m^2 (10 kTd) for helium, deviations from the Maxwellian form appeared. As seen in Fig. 4, the energy distributions for Ar^+ develop an enhanced high-energy tail for $E/N > 2\times10^{-17}$ V m^2. This deviation from a Maxwellian form was not evident in the earlier Ar^+ results of Radovanov and co-workers [10] because of a lack of detection sensitivity and severe limits on the maximum energies that could be observed in that work. For Ne^+ and He^+, the deviations from Maxwellian behavior are initially manifested by decreases in the ion flux at the low-energy ends of the distributions.

It is clear from the present results that, at sufficiently high E/N, the charge-transfer model fails to provide an adequate prediction of the kinetic-energy distributions for singly charged ions. It will be shown in Sec. IV B that the mean ion energies also begin to fall below the model predictions based on Eq. (9) or (10) when deviations from the Maxwellian form become evident. It should be noted that, in the case of helium, it was not possible to obtain reliable data on the ion kinetic-energy distributions for E/N above about 2.0×10^{-17} V m^2 (20 kTd) because of the inability to maintain a stable self-sustained Townsend discharge.

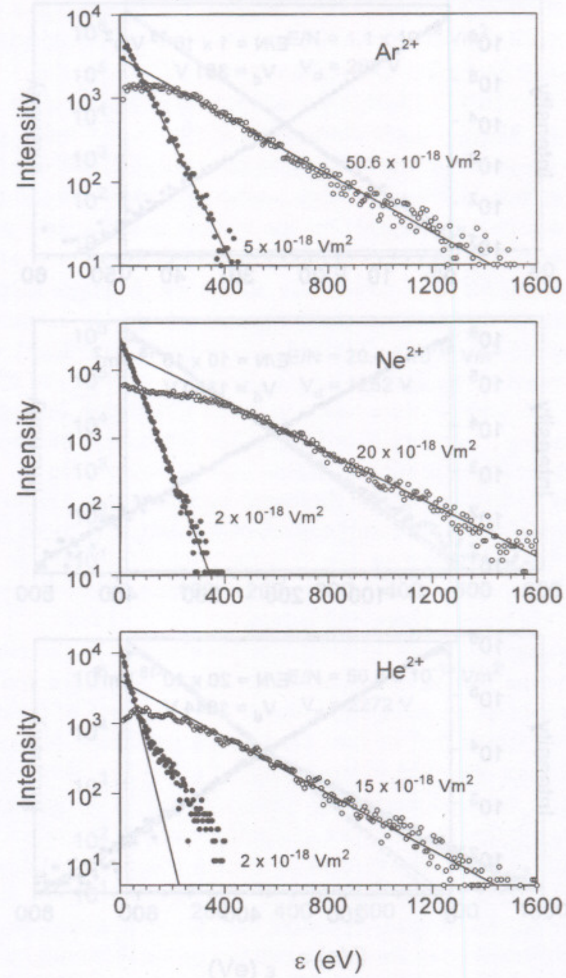

FIG. 7. Examples of the measured kinetic-energy distributions for the doubly charged ions Ar^{2+}, Ne^{2+}, and He^{2+} for a gap spacing of 2.0 cm and for the indicated values of E/N. The solid lines are Maxwellian fits to the data.

Examples of measured ion-energy distributions for the doubly charged ions Ar^{2+}, Ne^{2+}, and He^{2+} are shown in Fig. 7. The data presented in this figure were obtained for a gap spacing of 2 cm and at the indicated values for E/N. The solid lines are fits to the data of the form $a\exp(-b\varepsilon)$. For $E/N < 1.5\times10^{-17}$ V m^2, the Maxwellian form provides reasonable fits to the distributions for Ar^{2+} and Ne^{2+} ions. In the case of He^{2+}, the measured kinetic-energy distributions cannot be described adequately by a Maxwellian even at relatively low E/N values. Below about 1.0×10^{-17} V m^2, the He^{2+} distributions exhibit a two-temperature characteristic as seen by the data at $E/N = 0.2\times10^{-17}$ V m^2 in Fig. 7. At high E/N, the energy distributions for all three doubly charged ions tend to develop maxima at energies significantly greater than 5 eV, below which the flux is lower than expected for a Maxwellian. The extent to which the maxima in the observed energy distributions for doubly charged ions are real, e.g., are due to a breakdown of the one-dimensional approximation for ion transport, or are the consequence of instrumental effects due to low-energy ion discrimination is not known. However, from the results obtained for singly

TABLE I. Summary of the results for Ar^+. Listed for each value of E/N are the mean energy $\langle\varepsilon\rangle$ calculated using Eq. (11), the mean energy kT_+ from fits to the data using Eq. (6), the β parameter from fits to the data using Eq. (5), and $Q_{CT}=Q_0$ calculated from Eq. (7) using kT_+ from Maxwellian fits. Values for kT_+ in parentheses, apply only to the high-energy tail.

E/N (10^{-18} V m^2)	$\langle\varepsilon\rangle$ (eV)	kT_+ (eV)	β	Q_{CT} (10^{-16} cm^2)
1.0	1.90±0.50	2.30	−0.020	57.9
2.0	4.10±0.54	4.61	−0.015	48.8
5.0	11.62±0.59	12.50	0.010	43.0
10.1	25.0±2.8	26.0	−0.036	40.4
15.2	34.7±3.0	37.0	−0.021	43.8
20.4	38.5±6.0	43.0 (51.0)	−0.010	47.4
30.5	50.9±7.5	52.0 (69.0)	−0.040	58.7
50.6	70.4±10.6	70.0 (106.0)		72.3

charged ions, it would appear that effects of ion discrimination are not likely to extend up to energies greater than 50 eV as would be required to account for the deviations from Maxwellian behavior evident from the data in Fig. 7 at high E/N.

B. Mean energies

For each of the singly charged ions Ar^+, Ne^+, and He^+, no significant differences were found in the mean energies determined from fits to the measured energy-distribution data using Eqs. (9) and (10). Mean energies that were obtained from the use of Eqs. (10) and (11) are presented in Figs. 8–10 and also in Tables I–VI. For the data at high E/N that deviate from the Maxwellian form, the values for kT_+ were extracted from fits to the low-energy portions of the distributions as shown in Figs. 4–6. Maxwellian fits to the high-energy tails of the Ar^+ distributions yielded values for kT_+ indicated by the open diamond symbols in Fig. 8 and the numbers enclosed in parentheses in Table I. It is seen that the effective ion temperatures associated with the high-energy tails of the Ar^+ distributions for $E/N>2.0\times10^{-17}$ V m^2 are significantly greater than the temperatures associated with the low-energy parts of the distributions. Nevertheless, because only a small fraction of the ion flux is represented by the high-energy tail, it is found that, at all E/N, the values for kT_+ from the low-energy parts of the distributions are in good agreement with the corresponding values for $\langle\varepsilon\rangle$ calculated directly from the data using Eq. (11).

TABLE II. Summary of the results for Ne^+. Listed for each value of E/N are the mean energy $\langle\varepsilon\rangle$ calculated using Eq. (11), the mean energy kT_+ from fits to the data using Eq. (6), the β parameter from fits to the data using Eq. (5), and $Q_{CT}=Q_0$ calculated from Eq. (7) using kT_+ from Maxwellian fits.

E/N (10^{-18} V^2)	$\langle\varepsilon\rangle$ (eV)	kT_+ (eV)	β	Q_{CT} (10^{-16} cm^2)
0.36	1.53±0.30	1.47	−0.001	24.5
0.50	2.10±0.10	2.09	0.002	23.8
0.75	3.24±0.15	3.20	0.003	23.1
1.0	3.81±0.40	3.95	0.040	26.2
2.0	7.60±0.90	8.00	0.011	26.3
5.0	18.3±3.0	18.8	0.030	27.3
10.0	42.0±3.4	42.9	−0.020	23.8
15.0	57.1±4.8	56.3	−0.012	26.3
20.0	71.8±5.3	73.0	−0.040	27.9
30.0	90.6±9.1	92.0	−0.050	33.1
50.0	106.0±10.0	1.09		47.2

TABLE III. Summary of the results for He^+. Listed for each value of E/N are the mean energy $\langle\varepsilon\rangle$ calculated using Eq. (11) the mean energy kT_+ from fits to the data using Eq. (6), the β parameter from fits to the data using Eq. (5), and $Q_{CT}=Q_0$ calculated from Eq. (7) using kT_+ from Maxwellian fits.

E/N (10^{-18} V m^2)	$\langle\varepsilon\rangle$ (eV)	kT_+ (eV)	β	Q_{CT} (10^{-16} cm^2)
0.54	2.22±0.40	2.26	0.030	24.3
1.0	4.56±0.25	4.20	0.020	21.9
2.0	9.63±0.40	10.1	0.010	20.7
5.0	27.2±1.2	26.6	0.015	18.4
7.5	37.5±1.0	37.4	0.026	20.0
10.0	51.3±2.5	51.3	0.011	19.5
15.0	70.1±5.0	69.0	0.030	21.4
20.0	91.0±6.4	87.3	0.040	22.0

Shown in Figs. 8–10 are values for kT_+ (solid circles) estimated from the drift velocities, W_+, measured by Hornbeck [20] in a pulsed Townsend discharge experiment for $E/N<3.0\times10^{-18}$ V m^2. The estimates are based on the relationship

$$kT_+=\frac{\pi}{2}MW_+^2, \tag{15}$$

where M is the ion mass (see Ref. [10]). Also shown for Ar^+ and Ne^+ are values for kT_+ calculated from the drift velocities measured by Hegerberg and co-workers [32] in a drift-tube experiment (solid inverted triangles). Although the drift-velocity results appear to be consistent with the mean ion energies determined here, in all cases, the values from Hornbeck's data for Ar^+, Ne^+, and He^+ tend to fall somewhat below the present values. The results for Ar^+ and

TABLE IV. Summary of the results for Ar^{2+}. Listed for each value of E/N are the mean energy $\langle\varepsilon\rangle$ calculated using Eq. (11) and the fractional contribution to the total ion flux $R(Ar^{2+})$ calculated using Eqs. (12)–(14).

E/N (10^{-18} Vm^2)	$\langle\varepsilon\rangle$ (eV)	$R(Ar^{2+})$
1.0	9.5±2.7	0.015±0.005
2.0	19.2±2.0	0.016±0.005
5.3	66.3±9.1	0.007±0.002
10.1	125.0±17.0	0.007±0.002
15.2	162.0±24.0	0.010±0.003
20.4	178.0±22.0	0.008±0.002
30.0	224.0±34.0	0.010±0.003
50.0	245.0±37.0	0.010±0.003

TABLE V. Summary of the results for Ne^{2+}. Listed for each value of E/N are the mean energy $\langle\varepsilon\rangle$ calculated using Eq. (11); and the fractional contribution to the total ion flux $R(Ne^{2+})$ calculated using Eqs. (12)–(14).

E/N (10^{-18} V m^2)	$\langle\varepsilon\rangle$ (eV)	$R(Ne^{2+})$
0.36	7.8±0.8	0.011±0.002
0.50	10.8±1.1	0.014±0.003
0.75	14.8±0.8	0.017±0.004
1.0	20.9±0.9	0.020±0.006
2.0	41.5±2.1	0.022±0.006
5.0	82.7±4.1	0.012±0.010
10.1	180.0±25.0	0.015±0.003
15.2	210.0±33.0	0.016±0.004
20.0	270.0±30.0	0.018±0.007
30.0	294.0±44.0	0.019±0.006
50.0	326.0±49.0	

Ne^+ from Hegerberg and co-workers show better agreement with the present data for E/N below 1×10^{-18} V m^2.

Figure 8 also shows the mean energies for Ar^+ previously reported by Radovanov and co-workers [10] (open squares), which have been multiplied by the factor 0.67 (see the Appendix) to make them consistent with the definition of mean energy used here. Except at the highest value of E/N (2.0×10^{-17} V m^2), the earlier results agree with the present data to within the estimated uncertainties. The uncertainties in the present data are given in Tables I–VI and are comparable in most cases to the sizes of the data points that are shown. The uncertainties given in the tables reflect the range of values extracted from energy distributions measured at different times using different ion focusing and discharge conditions. The values listed in the tables and also plotted in Figs. 8–10 are those obtained under conditions for which there was greatest confidence in the uniformity of the ion transmission. The uncertainties in mean energy are less than ±15% in most cases. The main source of uncertainty in the data of Radovanov *et al.* [10], as reflected in the error bars shown in Fig. 8, was attributed to uncertainties in fitting the data. Because the present S_i versus ε_i data exhibit much less statistical scatter, this source of uncertainty has been significantly reduced.

For the singly charged ions, the solid straight lines are fits

TABLE VI. Summary of the results for He^{2+}. Listed for each value of E/N are the mean energy $\langle\varepsilon\rangle$ calculated using Eq. (11) and the fractional contribution to the total ion flux $R(He^{2+})$ calculated using Eqs. (12)–(14).

E/N (10^{-18} V m^2)	$\langle\varepsilon\rangle$ (eV)	$R(He^{2+})$
0.536	20.0±3.1	0.012±0.006
1.0	25.5±2.5	0.014±0.009
2.0	44.5±8.0	0.013±0.008
5.0	113.0±28.0	0.010±0.006
7.5	156.0±31.0	0.010±0.006
10.0	194.0±35.0	0.010±0.006
15.0	276.0±50.0	0.010±0.006
20.0	320.0±63.0	0.010±0.006

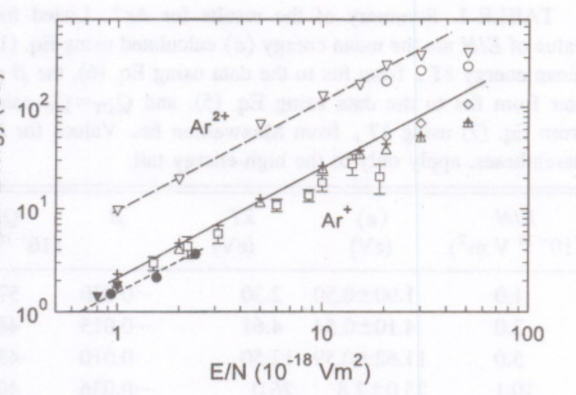

FIG. 8. Mean kinetic energy versus E/N for Ar^+ and Ar^{2+} in Ar. The crosses are values for kT_+ obtained from Maxwellian fits to the energy distribution data and the open triangles are values for $\langle\varepsilon\rangle$ calculated using Eq. (11). The open diamonds correspond to fits to the high-energy tails of the distributions in those cases where there was a significant deviation from Maxwellian behavior. The results for Ar^+ are compared with the data of Ref. [10] (open squares) and estimates from the drift velocity data in Ref. [20] (solid circles) and in Ref. [32] (solid inverted triangles). The lines are fits to the data based on an assumed direct proportionality between $\langle\varepsilon\rangle$ and E/N. For Ar^{2+}, the open inverted triangles are mean energies calculated using Eq. (11) and the open circles are ion temperatures from Maxwellian fits to the high-energy part of the energy distributions.

to the data that are consistent with the direct proportionality between kT_+ and E/N implied by Eq. (7), i.e., they have a slope of 1.0 on a log-log plot. It is seen, especially for Ar^+ and Ne^+, that above 2.0×10^{-17} V m^2, where the kinetic-energy distributions become non-Maxwellian, the values for kT_+ and $\langle\varepsilon\rangle$, indicated respectively by the crosses and open,

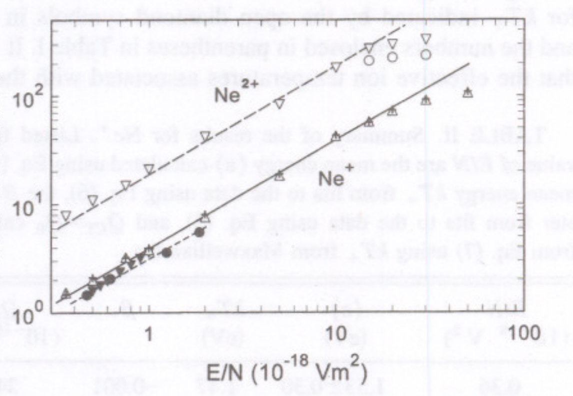

FIG. 9. Mean kinetic energy versus E/N for Ne^+ and Ne^{2+} in Ne. The crosses are values for kT_+ obtained from Maxwellian fits to the energy distribution data and the open triangles are values for $\langle\varepsilon\rangle$ calculated using Eq. (11). The results for Ne^+ are compared with estimates from the drift velocity data in Ref. [20] (solid circles) and in Ref. [32] (solid inverted triangles). The lines are fits to the data based on the assumption of a direct proportionality between $\langle\varepsilon\rangle$ and E/N. For Ne^{2+}, the open inverted triangles are mean energies calculated using Eq. (11) and the open circles are ion temperatures from Maxwellian fits to the high-energy part of the energy distributions.

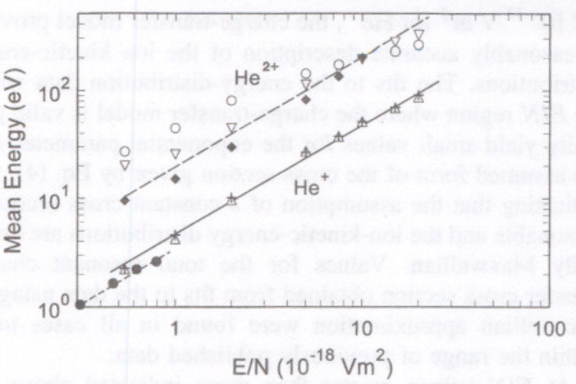

FIG. 10. Mean kinetic energy versus E/N for He^+ and He^{2+} in He. The crosses are values for kT_+ obtained from Maxwellian fits to the energy distribution data and the open triangles are values for $\langle\varepsilon\rangle$ calculated using Eq. (11). The results for He^+ are compared with estimates based on the drift velocity data in Ref. [20] (solid circles). The solid line is a fit to the He^+ data based on a direct proportionality between $\langle\varepsilon\rangle$ and E/N. For He^{2+}, the open inverted triangles are mean energies calculated using Eq. (11), the open circles are ion temperatures from Maxwellian fits to the high-energy part of the distributions, and the solid diamonds are temperatures from Maxwellian fits to the low-energy part.

upright triangles, begin to fall below the line. However, for Ar^+, the drop in mean energy is not as great as implied by the earlier data of Radovanov and co-workers [10] at $E/N \simeq 2\times10^{-17}$ V m^2.

The mean energies for the doubly charged ions indicated by the open inverted triangles in Figs. 8–10 and given in Tables IV–VI are derived from the data using Eq. (11). The open circles correspond to the ion temperatures implied by Maxwellian fits to the high energy portions of the energy-distribution data as seen in Fig. 7. In the case of He, the solid diamonds correspond to the temperatures implied by the low-energy portions of the energy distributions. For all three gases, the mean energies of the doubly charged ions are significantly greater than the mean energies of the singly charged ions at any given E/N. The data for Ar^{2+} and Ne^{2+} show a direct proportionality between $\langle\varepsilon\rangle$ and E/N below about 1.5×10^{-17} V m^2, as indicated by the large dashed lines in Figs. 8 and 9 that have a slope of 1.0.

C. Abundances of doubly charged ions

The relative contributions to the total flux of ions hitting the cathode from the doubly charged species Ar^{2+}, Ne^{2+}, and He^{2+} were estimated at each E/N using Eqs. (12)–(14). The results are given in Tables IV–VI together with estimated uncertainties (typically less than $\pm30\%$) based on data obtained using different ion focusing conditions. The results for $R(Ar^{2+})$ are also shown in Fig. 11. There is a tendency in all three gases for the contributions from the doubly charged ions to initially decrease with E/N and then remain relatively constant. The $R(Ar^{2+})$ data are also consistent in magnitude with the values reported by Radovanov and co-workers [10]. In no case were the ions Ar^{2+}, Ne^{2+}, and He^{2+} found to constitute more than 3% of the total ion flux.

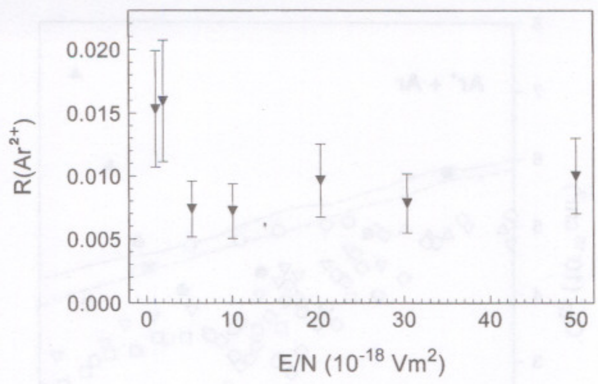

FIG. 11. Dependence of the relative contribution of Ar^{2+} to the total ion flux in argon on E/N.

D. Charge-transfer cross sections

From fits to the kinetic-energy distribution data using the Maxwellian form given by Eq. (6), effective constant charge-transfer cross sections can be extracted from the adjustable parameter b using Eq. (7), i.e.,

$$Q_{CT}=Q_0=eb\left(\frac{E}{N}\right). \tag{16}$$

The question can therefore be raised about the extent to which the values derived from Eq. (16) are consistent with the available information about the total resonant charge-transfer cross sections in the relevant range of energies centered about the experimentally determined mean energies. Values for Q_{CT} determined from Eq. (16) for Ar^+ + Ar, Ne^+ + Ne, and He^+ + He are given in Tables I–III. These values are also plotted versus $\langle\varepsilon\rangle$ in Figs. 12–14 together with selected cross-section data from numerous sources [30,33–47] that were extracted from the compilations published by Phelps [30], Sakabe and Izawa [33], and Martinez and Dheandhanoo [34]. The values for Q_{CT} that apply to the data at low E/N where the Maxwellian form adequately describes the entire energy distribution are indicated by the closed circles in Figs. 12–14. The closed triangles correspond to the cases at high E/N where the distributions deviate from the Maxwellian form. In these cases, Q_{CT} were derived from fits to the low-energy parts of the distributions as discussed above. The data from other sources are indicated by lines or open symbols.

In those cases where the Maxwellian form accurately describes the measured energy distributions for Ar^+, Ne^+, and He^+, it is seen that the cross-section values derived from the data are consistent with the available data and do not vary significantly with $\langle\varepsilon\rangle$. The cross sections obtained from distributions that deviate from Maxwellian form tend, in all cases, to have values that increase with $\langle\varepsilon\rangle$ and lie above those reported in previously published works.

V. DISCUSSION AND CONCLUSIONS

It is possible from the present experimental results to determine the range of E/N within which the simple charge-transfer model for ion transport is valid. For E/N below about 2×10^{-17} V m^2 for Ar^+ and Ne^+ and below

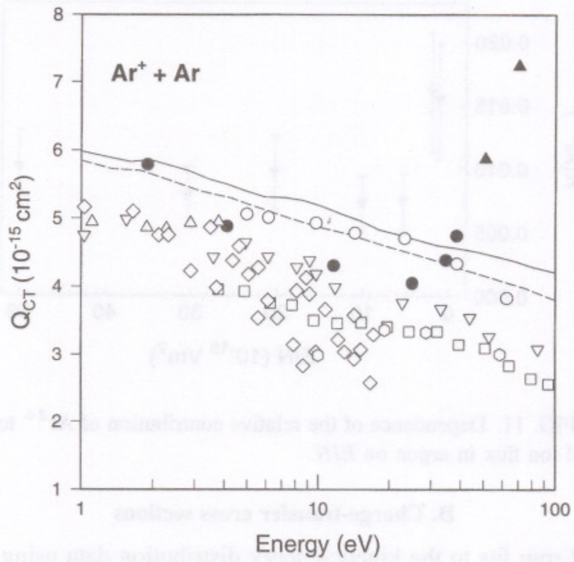

FIG. 12. Values for Q_{CT} from Maxwellian fits to the Ar^+ data versus $\langle \varepsilon \rangle$ (closed symbols) compared with the $Ar^+ + Ar$ charge-transfer cross sections from the following sources: Ref. [33], solid line; Ref. [30], dashed line; Ref. [34], open circles; Ref. [35], open squares; Ref. [41], open triangles; Ref. [37], open inverted triangles; Ref. [38], open diamonds; and Ref. [39], open hexagons. The closed circles correspond to cases where the energy distributions were Maxwellian and the closed triangles to cases where there were deviations from Maxwellian behavior.

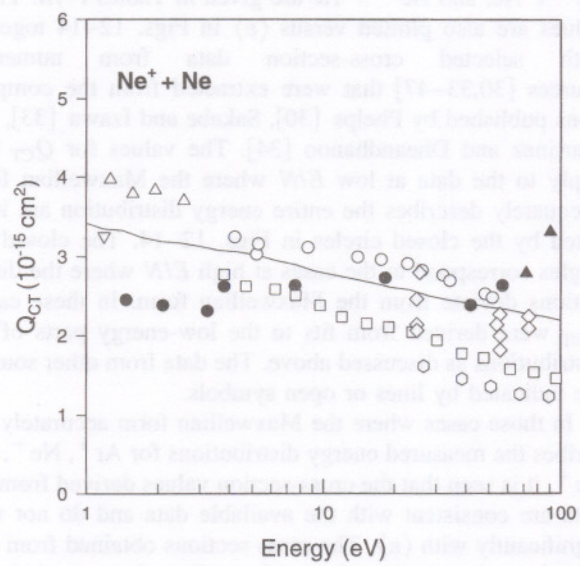

FIG. 13. Values for Q_{CT} from Maxwellian fits to the Ne^+ data versus $\langle \varepsilon \rangle$ (closed symbols) compared with the $Ne^+ + Ne$ charge-transfer cross sections from the following sources: Ref. [33], solid line; Ref. [34], open circles; Ref. [35], open squares; Ref. [40], open triangles; Ref. [41], open inverted triangles, Ref. [42], open diamonds, and Ref. [43], open hexagons. The closed circles correspond to cases where the energy distributions were Maxwellian and the closed triangles to cases where there were deviations from Maxwellian behavior.

1×10^{-17} V m^2 for He^+, the charge-transfer model provides a reasonably accurate description of the ion kinetic-energy distributions. The fits to the energy-distribution data within the E/N region where the charge-transfer model is valid generally yield small values for the exponential parameter β in the assumed form of the cross section given by Eq. (4), thus indicating that the assumption of a constant cross section is reasonable and the ion-kinetic-energy distributions are essentially Maxwellian. Values for the total resonant charge-transfer cross section obtained from fits to the data using the Maxwellian approximation were found in all cases to lie within the range of previously published data.

At E/N values greater than those indicated above, the measured ion-kinetic-energy distributions begin to deviate from the Maxwellian form predicted by the charge-transfer model. These deviations are manifested in the case of Ar^+ by the appearance of enhanced high-energy tails and for Ne^+ and He^+ by suppressions in the low-energy end of the distributions. It is also significant that when the energy distributions deviate from Maxwellian form, the cross sections determined from the Maxwellian fits take on values for all three ions that are significantly greater than suggested by the available data. This means that the ion temperatures are lower than would be predicted by the charge-transfer model. This trend is reflected in the data on mean ion energies that exhibit significant departures from the simple proportionality $\langle \varepsilon \rangle \propto E/N$ implied by the model at E/N values where the energy distributions are non-Maxwellian.

It is not presently known why the observed ion-kinetic-energy distributions depart from the predictions of the charge-transfer model at high E/N. Although it can be speculated, at least for Ar^+, that the non-Maxwellian behav-

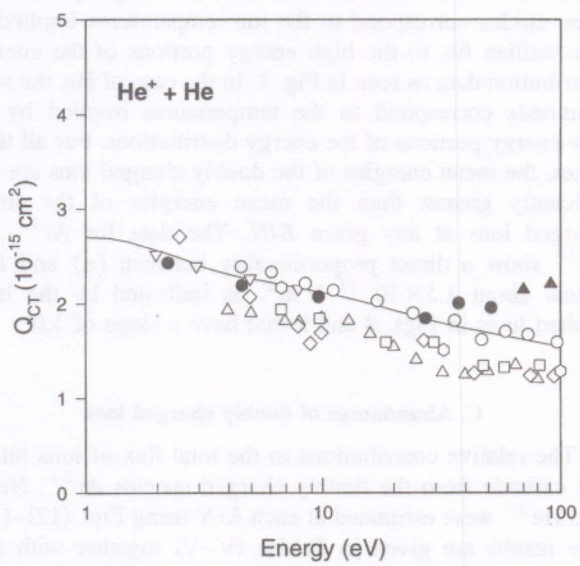

FIG. 14. Values for Q_{CT} from Maxwellian fits to the He^+ data versus $\langle \varepsilon \rangle$ (closed symbols) compared with the $He^+ + He$ charge-transfer cross sections from the following sources: Ref. [33], solid line; Ref. [44], open circles; Ref. [36], open triangles; Ref. [47], open squares; Ref. [45], open inverted triangles, Ref. [37], open diamonds, and Ref. [46], open hexagons. The closed circles correspond to cases where the energy distributions were Maxwellian and the closed triangles to cases where there were deviations from Maxwellian behavior.

ior at high E/N is attributable to deviations from equilibrium conditions in the transport of ions, there is neither unequivocal experimental evidence nor theoretical arguments to support this speculation. The measured ion-energy distributions did not, for example, depend significantly on the electrode gap spacing and the maximum observable ion energies failed to come close to the upper limit eV_d imposed by voltage drop across the electrodes as recently seen in the case of H^+ transport in H_2 discharges [48].

The mean free path of the ions is estimated, in all cases, to be small compared with the electrode gap spacing. For example, in the case of Ar^+ in Ar, the mean free path varies from about 3×10^{-3} cm at the lowest E/N to about 4×10^{-2} cm at the highest E/N. Because the mean free path is generally more than an order of magnitude smaller than the gap spacing, it can be argued that there should always be a sufficient number of collisions to ensure equilibrium.

Of course, arguments based on mean free path considerations or possible changes in the energy distribution with gap spacing must necessarily also consider the energy dependence of the cross section and the density distribution of ions in the gap. The resonant charge-transfer cross sections for the ions Ar^+, Ne^+, and He^+ decrease only relatively slowly with energy up to about 10^5 eV, at which point they drop precipitously [33]. A slow decrease in the cross section with energy presents an unfavorable condition for the occurrence of deviations from equilibrium that are manifested by the appearance of high-energy "runaway" ions.

It is conceivable that apparent deviations from equilibrium could be reflected in the data if a significant fraction of the ions were formed within one mean-free-path distance from the cathode. However, because of the electron avalanching effect in a Townsend discharge, the ion densities are expected to be the highest near the anode. It has been argued [49] that even at E/N as high as 4×10^{-17} V m^2 (40 kTd), the rate of ion formation by electron impact in an argon discharge is nearly independent of position within the electrode gap.

Although inelastic collisions that result in electronic excitation or ionization begin to occur at energies above 20 eV, it is found [31,49], at least in the case of Ar^+ + Ar, that the cross sections for these processes are an order of magnitude or more below that for charge transfer, even for energies up to 500 eV. It was previously shown by Radovanov and coworkers [10] that ion-energy loss by processes other than charge transfer are not likely to affect significantly the transport of Ar^+ in Ar for E/N up to 2×10^{-17} V m^2. The extent to which inelastic ion-atom collisions resulting in excitation or ionization cause a breakdown of the charge-transfer model at E/N above 2×10^{-17} V m^2 remains unclear. Collisions of ions with long-lived metastable excited atoms may also be important at high E/N, but little or nothing is known about the cross sections or rates for these processes.

Deviations from Maxwellian behavior at low ion energies may reflect in part a failure of the one-dimensional approximation. This approximation neglects effects due to momentum transfer and angular distributions of the ions that may be characteristic of the relevant ion-molecule interactions. It is expected that angular scattering will be most significant at the lowest energies and could lead to an apparent suppression or reduction in the ion flux at these energies.

The mean kinetic energies of the doubly charged ions Ar^{2+}, Ne^{2+}, and He^{2+} were found to be much higher than the mean energies of the corresponding singly charged ions. This trend suggests that charge-transfer or inelastic collisons are comparatively less important as energy-loss mechanisms in affecting the transport of doubly charged ions. From the experimental results of Huber [50], it appears that the cross section for the double electron transfer process

$$Ar^{2+}(3s^23p^4)+Ar(3s^23p^6) \rightarrow Ar(3s^23p^6)+Ar^{2+}(3s^23p^4) \quad (17)$$

at collision energies below 1000 eV is nearly an order of magnitude below the cross section for Ar^+ + Ar charge transfer. (Also see [4] for a review of the double charge-transfer processes in argon). If the charge-transfer model applies to Ar^{2+} + Ar, i.e., if process (17) above dominates, then, based on Eq. (7), the lower cross section for double charge transfer compared to single charge transfer in Ar^+ + Ar collisions would account for the higher mean energies observed for Ar^{2+}. It is found experimentally [50] that in the energy range relevant to the E/N values considered here, the cross sections for the competing processes

$$Ar^{2+}(3s^23p^4)+Ar(3s^23p^6)\rightarrow 2Ar^+(3s^23p^5,{}^2P) \quad (18)$$

and

$$Ar^{2+}(3s^23p^4)+Ar(3s^23p^6)\rightarrow Ar^{+*}(3s^3p^6,{}^2S)+Ar^+ \quad (19)$$

are more than an order of magnitude below that of process (17). Thus the present results appear to be consistent with a simple charge-transfer model for transport of Ar^{2+} in Ar. This presumes, of course, that the kinetic-energy distributions are really Maxwellian and that the deviations from Maxwellian form that appeared here at low energies are associated either with instrumental ion-discrimination effects or a possible breakdown of the one-dimensional approximation assumed in the model. The mean energy data for Ar^{2+} in Table IV, when used in the simple charge-transfer model, yield total cross sections for process (17) that lie in the range of 9.0×10^{-16} to 10.6×10^{-16} cm^2. This range of values agrees, to within the stated uncertainties, with extrapolations to low energies of the data from Huber [50] and from Cosby and Moran [51].

From an examination of available cross-section data [52–55], it would appear that similar arguments could be made for the other doubly charged ions Ne^{2+} and He^{2+}. However, unlike Ar^{2+} and Ne^{2+}, the energy distribution data for He^{2+} are not consistent with the charge-transfer model within the E/N range covered in this work. In the case of Ne^{2+}, the data given in Table V imply a total double charge-transfer cross section in the range 4.7×10^{-16}–6.7×10^{-16} cm^2.

The relative contributions of the doubly charged ions to the total ion fluxes impinging on the cathode were found to be small (less than 3% at all E/N). The tendency for the doubly charged ion contributions to decrease and become constant with increasing E/N is not understood. This trend would seem to be contrary to expectations based on the rates for ion formation by electron impact. When E/N increases, the mean energy of electrons in the discharge should increase and thereby cause a corresponding increase in the relative rate for doubly charged ion production consistent with the known energy dependences of the cross sections for single and double ionization by electron impact [56]. There is no evidence based on the energy dependence of the cross sections [50] that the rates for destruction of doubly charged ions, such as by processes (18) and (19), should significantly increase with increasing E/N. Collisions involving metastable excited species, e.g., $He^{2+} + He(2\,^3S)$, could become important at high E/N due to an increase in the metastable density; however, nothing is known about either the densities of metastable species or the effectiveness of these types of collisions in destroying doubly charged ions. It might be speculated that processes such as (18) and (19), above in which doubly charged ions are converted to singly charged ions, could influence the shapes of the energy distributions for Ar^+, Ne^+, and He^+. In particular, this source of singly charged ions in the discharge might contribute significantly to the high-energy tails seen in the Ar^+ distributions at relatively high E/N.

It is also of interest to point out that the dimer ions Ar_2^+, Ne_2^+, and He_2^+ were sometimes observed, albeit at very low abundances, for values of E/N below about 1.0×10^{-18} V m^2. At higher E/N, these ions were not detected. Although the dimer ions can presumably be formed even at low pressures and high E/N by the associative ionization mechanism [57], e.g.,

$$He^* + He \rightarrow He_2^+ + e, \tag{20}$$

the failure to see them implies that either the rates for formation are very low and/or they are readily destroyed by collisions [58].

ACKNOWLEDGMENTS

This work was supported by and performed in the Electricity Division, Electronics and Electrical Engineering Laboratory, National Institute of Standards and Technology, Technology Administration, U.S. Department of Commerce. The authors are grateful for valuable discussions and suggestions from S. B. Radovanov, University of New Mexico; A. V. Phelps and B. M. Jelenkovic, JILA; Y. Wang, University of Notre Dame; and J. Bretagne, T. Simko, and G. Gousset, Université Paris–Sud.

APPENDIX

Consideration is given here to the problem of selecting the correct functional form to fit measured data on ion-energy distributions in order to make proper comparisons with the predictions of theoretical models such as based on solutions of the Boltzmann transport equation. In the discussion that follows, it will be assumed that the correct one-dimensional velocity distribution is that which corresponds to a solution of the Boltzmann transport equation for motion of ions in a high, uniform electric field. The approximation considered is one-dimensional in the sense that angular scattering and motion of the ions in a direction perpendicular to the electric-field direction are neglected (see, for example, Ref. [59]). If it is also assumed that resonant symmetric charge transfer is the only collision process with a velocity-dependent cross section $Q_{CT}(v_z)$, it can then be shown [10,11,31] that the one-dimensional velocity distribution assumes the form

$$g(v_z)dv_z = C_1 \exp\left[-\left(\frac{eE}{MN}\right)^{-1}\int_0^{v_z} v_z' Q_{CT}(v_z')dv_z'\right]dv_z, \tag{A1}$$

where M is the ion mass and v_z is the velocity component in the direction of the electric field. Considering first the approximation of a constant cross section, one obtains from Eq. (A1) the Maxwellian form

$$g(v_z) = C_1 \exp(-mv_z^2/2kT_+), \tag{A2}$$

where kT_+ is defined by Eq. (7). The equivalent energy distribution $f(\varepsilon)$ is obtained from the transformation

$$f(\varepsilon)d\varepsilon = g(v_z)\frac{\partial v_z}{\partial \varepsilon}d\varepsilon, \tag{A3}$$

which gives

$$f(\varepsilon)d\varepsilon = C_1(2M\varepsilon)^{-1/2}\exp(-\varepsilon/kT_+)d\varepsilon. \tag{A4}$$

Note that the transformation given by Eq. (10) in Ref. [10] contains an error in the omission of the factor $\varepsilon^{-1/2}$.

From the normalization requirement

$$\int_0^\infty f(\varepsilon)d\varepsilon = 1 \tag{A5}$$

it is found that $C_1 = (2M)^{1/2}/(\pi kT_+)^{1/2}$. The "true" mean energy $\langle\varepsilon\rangle_t$ obtained using the distribution $f(\varepsilon)$ is given by

$$\langle\varepsilon\rangle_t = \int_0^\infty \varepsilon f(\varepsilon)d\varepsilon = \tfrac{1}{2}kT_+, \tag{A6}$$

which differs by the factor 1/2 from the definition of mean energy used here, Eq. (10), which is based on a measured flux-energy distribution.

If, *as in the present experiments*, one measures ion energies using an energy or velocity selector, then one is not directly measuring the true energy distribution $f(\varepsilon)$, but rather a flux-energy distribution [15]. The shape of the flux-energy distribution that is recorded depends on the type of energy or velocity analysis that is employed. The experiments discussed in the present work were performed under conditions where the ions pass through an electrostatic energy selector with a fixed energy spread $\Delta\varepsilon_r$ that is independent of the recorded nominal energy ε_i. Therefore, the signals $S_i(\Delta\varepsilon_r, \varepsilon_i)$ recorded at each ε_i represent a differential flux that corresponds to the numbers of ions with kinetic energies in the range $\varepsilon_i - \Delta\varepsilon_r/2$ to $\varepsilon_i + \Delta\varepsilon_r/2$ that cross a fixed area in the planar cathode per unit time. Here the area is defined by the sampling orifice and the analyzer transmission function is assumed, for simplicity, to be rectangular. In reality the transmission function is more likely to be Gaussian as discussed below.

Allowing that, in velocity space, the flux is proportional to $v_z g(v_z)dv_z$ (see Ref. [15]), it can be shown that for a rectangular transmission function and an assumed Maxwellian form for $f(\varepsilon)$ [Eq. (A4) above], one obtains

$$S_i(\Delta\varepsilon_r,\varepsilon_i)=n_oA(\pi kT_+)^{-1/2}\int_{\varepsilon_i-\Delta\varepsilon_r/2}^{\varepsilon_i+\Delta\varepsilon_r/2}\left(\frac{2\varepsilon}{M}\right)^{1/2}\varepsilon^{-1/2}\times\exp\left(-\frac{\varepsilon}{kT_+}\right)d\varepsilon, \quad (A7)$$

where n_oA is an intensity-geometrical factor proportional to the area of the sampling orifice and the density of ions at the orifice. Integration of this equation gives

$$S_i(\Delta\varepsilon_r,\varepsilon_i)=n_oA\left(\frac{2}{\pi MkT_+}\right)^{1/2}G(\Delta\varepsilon_r)\exp\left(-\frac{\varepsilon_i}{kT_+}\right), \quad (A8)$$

where

$$G(\Delta\varepsilon_r)=\exp\left(\frac{\Delta\varepsilon_r}{2kT_+}\right)-\exp\left(\frac{-\Delta\varepsilon_r}{2kT_+}\right) \quad (A9)$$

or

$$G(\Delta\varepsilon_r)\simeq\frac{\Delta\varepsilon_r}{kT_+}+\frac{1}{6}\left(\frac{\Delta\varepsilon_r}{kT_+}\right)^3+\cdots \quad (A10)$$

if $\Delta\varepsilon_r/kT_+<1$. It is seen that the signal is roughly proportional to $\Delta\varepsilon_r$ as expected. The signal given by Eqs. (A8)–(A10) has the form $a\exp(-b\varepsilon)$ for the flux-energy distribution [Eq. (6)] that was used to fit the measured kinetic-energy-distribution data in the present work.

In the more general situation of an arbitrary transmission function $p(\varepsilon,\varepsilon_i,\Delta\varepsilon_r)$ of "width" $\Delta\varepsilon_r$, Eq. (A7) should be replaced in the Maxwellian case with

$$S_i(\Delta\varepsilon_r,\varepsilon_i)=n_oA(2\pi kT_+/M)^{-1/2}\times\int_0^\infty p(\varepsilon,\varepsilon_i,\Delta\varepsilon_r)\exp\left(-\frac{\varepsilon}{kT_+}\right)d\varepsilon. \quad (A11)$$

If the transmission function is Gaussian, then

$$p(\varepsilon,\varepsilon_i,\Delta\varepsilon_r)\sim\exp[-\alpha(\varepsilon-\varepsilon_i)^2/\Delta\varepsilon_r^2], \quad (A12)$$

where $\alpha=2.771$ is the appropriate factor required for $\Delta\varepsilon_r$ to be the full width at half maximum. Provided $\varepsilon_i\gg\Delta\varepsilon_r$, the transmission function does not significantly distort the flux-energy distribution and the form $a\exp(-b\varepsilon)$ should still provide an acceptable representation of the data. However, as ε_i becomes comparable to or smaller than $\Delta\varepsilon_r$, the shape of the measured distribution becomes increasing governed by the form of $p(\varepsilon,\varepsilon_i,\Delta\varepsilon_r)$.

If the measurements are performed using a *velocity selector* with a rectangular transmission function, then the recorded signals are given by

$$S_i=C_2\int_{v_i-\Delta v/2}^{v_i+\Delta v/2}v_zg(v_z)dv_z, \quad (A13)$$

where C_2 is a constant and Δv is the constant velocity resolution centered about a recorded velocity v_i. In the case of a Maxwellian form, integration of this equation yields

$$S_i=C_2\left(\frac{kT_+}{m}\right)G'(v_i,\Delta v)\exp(-Mv_i^2/2kT_+), \quad (A14)$$

where

$$G'(v_i,\Delta v)=\exp\left(-\frac{M\Delta v^2}{8kT_+}\right)\left[\exp\left(\frac{Mv_i\Delta v}{2kT_+}\right)-\exp\left(-\frac{Mv_i\Delta v}{2kT_+}\right)\right]. \quad (A15)$$

For sufficiently high velocity and velocity resolution such that $v_i\Delta v/kT_+\ll1$, one obtains, after appropriate change of variable, a flux-energy distribution of the form $a\varepsilon^{1/2}\exp(-b\varepsilon)$. This is the form that gave the best fit to the data in Ref. [10] and gives a mean flux energy of $3kT_+/2$. This is also the form obtained for a standard three-dimensional Maxwellian distribution [29]. Although reasonable fits to the present data were sometimes obtained using this form, it was found that this happened under conditions where effects of low-energy ion discrimination were most evident. In any case, this is not the proper form to use for comparing the present data with the model predictions.

It should also be pointed out, as discussed by Allen [29], that if an energy analyzer is used for which the ratio $\Delta\varepsilon_r/\varepsilon$ is a constant instead of $\Delta\varepsilon_r$ (see Ref. [50]), then the recorded flux will be proportional to ε_i. In this case the appropriate fit to the data for a Maxwellian should be of the form $a\varepsilon\exp(-b\varepsilon)$. In no case were the present data adequately represented by this form.

Finally, if the charge-transfer cross section has the energy dependence given by Eq. (4), it is found after performing the integration in Eq. (A1) and making the transformation to the energy variable that

$$f(\varepsilon)d\varepsilon=C'(2M\varepsilon)^{-1/2}\exp\left[-\frac{\varepsilon^{1-\beta}}{kT_+(1-\beta)}\right]d\varepsilon. \quad (A16)$$

The form given by Eq. (5) is obtained using Eq. (A16) in Eq. (1) and requiring the normalization implied by Eq. (3). The factor C' is determined by the normalization requirement for $f(\varepsilon)$.

[1] C. Wild and P. Koidl, J. Appl. Phys. **69**, 2909 (1991).

[2] J. K. Olthoff, R. J. Van Brunt, S. B. Radovanov, J. A. Rees, and R. Surowiec, J. Appl. Phys. **75**, 115 (1994).

[3] J. Janes and C. Huth, J. Vac. Sci. Techol. A **10**, 3522 (1992).

[4] A. V. Phelps, J. Appl. Phys. **76**, 747 (1994).

[5] R. T. Farouki, S. Hamaguchi, and M. Dalvie, Phys. Rev. A **44**, 2664 (1991).

[6] R. M. Chaudhri and M. L. Oliphant, Proc. R. Soc. London Ser. A **137**, 662 (1932).

[7] W. D. Davis and T. A. Vanderslice, Phys. Rev. **121**, 219 (1963).

[8] I. Abril, A. Gras-Morti, and J. A. Vallés-Abarca, Phys. Rev. A **28**, 3677 (1983).

[9] J. E. Lawler, Phys. Rev. A **32**, 2977 (1985).

[10] S. B. Radovanov, R. J. Van Brunt, J. K. Olthoff, and B. M. Jelenkovic, Phys. Rev. E **51**, 6036 (1995).
[11] G. H. Wannier, *Statistical Physics* (Wiley, New York, 1966), pp. 462–466.
[12] I. M. Kagan and V. I. Perel, Doklady Akad. Nauk SSSR **98**, 575 (1954) [Sov. Phys. Dokl. **98**, 575 (1954)].
[13] H. Mase, T. Tanabe, K. Taneko, and G. Miyamoto, J. Phys. D **12**, L123 (1979).
[14] P. P. Ong and M. J. Hogan, J. Phys. B **18**, 1897 (1985).
[15] H. R. Skullerud and S. Holmstrom, J. Phys. D **18**, 2375 (1985).
[16] S. L. Lin and J. N. Bardsley, J. Phys. B **8**, L461 (1975).
[17] B. N. Klyarfield, L. G. Guseva, and A. S. Pokrovskaya-Soboleva, Zh. Tekh. Fiz. **36**, 704 (1966) [Sov. Phys. Tech. Phys. **11**, 520 (1966)].
[18] V. I. Kolobov and A. Fiala, Phys. Rev. E **50**, 3018 (1994).
[19] M. J. Druyvesteyn and F. M. Penning, Rev. Mod. Phys. **12**, 87 (1940).
[20] J. A. Hornbeck, Phys. Rev. **84**, 615 (1951).
[21] M. V. V. S Rao, R. J. Van Brunt, and J. K. Olthoff, Bull. Am. Phys. Soc. **40**, 1549 (1995).
[22] J. K. Olthoff, R. J. Van Brunt, and S. B. Radovanov, J. Res. Natl. Inst. Stand. Tech. **100**, 383 (1995).
[23] J. K. Olthoff, R. J. Van Brunt, and S. B. Radovanov, Appl. Phys. Lett. **67**, 473 (1995).
[24] Z. Lj. Petrovic and A. V. Phelps, Phys. Rev. E **47**, 2806 (1993); A. V. Phelps, Z. Lj. Petrovic, and B. M. Jelenkovic, *ibid.* **47**, 2825 (1993).
[25] K. G. Emeleus, Z. Phys. **268**, 175 (1974).
[26] D. Bhasavanich and A. B. Parker, Proc. R. Soc. London Ser. A **358**, 385 (1977).
[27] R. Schade, Z. Phys. **108**, 353 (1938); H. Büttner, *ibid.* **111**, 750 (1939).
[28] A. V. Phelps, in *Proceedings of the 22nd International Conference on Phenomena in Ionized Gases, Hoboken, 1995*, edited by K. H. Becker, W. E. Carr, and E. E. Kunhardt (Stevens Institute of Technology, Hoboken, NJ, 1995), Vol. 2, pp. 107–108.
[29] J. E. Allen, J. Phys. D **25**, 1839 (1992).
[30] A. V. Phelps, J. Phys. Chem. Ref. Data **20**, 557 (1991).
[31] H. R. Skullerud, J. Phys. B **2**, 86 (1969).
[32] R. Hegerberg, M. T. Elford, and H. R. Skullerud, J. Phys. B **15**, 797 (1982).
[33] S. Sakabe and Y. Izawa, At. Data Nucl. Data Tables **49**, 257 (1991); Phys. Rev. A **45**, 2086 (1992).
[34] R. I. Martinez and S. Dheandhanoo, J. Res. Natl. Bur. Stand **92**, 229 (1987); Int. J. Mass Spectrom. Ion Processes **74**, 241 (1986).
[35] W. H. Cramer, J. Chem. Phys. **28**, 688 (1958); **30**, 641 (1959).
[36] W. H. Cramer and J. H. Simons, J. Chem. Phys. **26**, 1272 (1957).
[37] P. Mahadevan and G. P. Magnuson, Phys. Rev. **171**, 103 (1968).
[38] B. J. Nichols and F. C. Witteborn, NASA Technical Report No. NASA TN D-3625, 1966 (unpublished).
[39] A. Rostagni, Nuovo Cimento **15**, 117 (1939).
[40] Y. Kaneko, N. Kobayashi, and I. Kanomata, J. Phys. Soc. Jpn. **27**, 992 (1969).
[41] N. Kobayashi, Mass Spectrom. **20**, 123 (1972); J. Phys. Soc. Jpn. **38**, 519 (1975).
[42] F. Wolf, Ann. Phys. (Leipzig) **30**, 313 (1937).
[43] A. Galli, A. Giardini-Guidoni, and G. G. Volpi, Nuovo Cimento **26**, 845 (1962).
[44] H. C. Hayden and N. G. Utterback, Phys. Rev. **135**, A1575 (1964).
[45] H. Helm, J. Phys. B **10**, 3683 (1977).
[46] F. J. de Heer, J. van Eck, and J. Kistemaker, in *Proceedings of the Sixth International Conference on Phenomena in Ionized Gases, Paris, 1963* (SERMAI, Paris, 1963), Vol. 1, p. 73. The cross sections shown are those tabulated in Sakabe and Izawa, Ref. [33].
[47] V. A. Belyaev, B. G. Brezhnev, and E. M. Erastov, Zh. Éksp. Teor. Fiz. **54**, 1720 (1968) [Sov. Phys. JETP **27**, 924 (1968)].
[48] M. V. V. S Rao, R. J. Van Brunt, J. K. Olthoff, Y. Wang, and R. L. Champion, Bull. Am. Phys. Soc. **40**, 1557 (1995).
[49] A. V. Phelps and B. M. Jelenkovic, Phys. Rev. A **38**, 2975 (1988).
[50] B. A. Huber, J. Phys. B **13**, 809 (1980).
[51] P. C. Cosby and T. F. Moran, J. Chem. Phys. **57**, 3569 (1972).
[52] H. Shrey and B. Huber, Z. Phys. A **273**, 401 (1975).
[53] W. B. Maier and B. Stewart, J. Chem. Phys. **68**, 4228 (1978).
[54] V. V. Afrosimov, G. A. Leiko, Yu. A. Mamaev, and M. N. Panov, Zh. Éksp. Teor. Fiz. **67**, 1329 (1974) [Sov. Phys. JETP **40**, 661 (1975)].
[55] R. D. Rivarola and R. D. Piacentini, Phys. Rev. A **20**, 1816 (1979).
[56] L. K. Kieffer and G. H. Dunn, Rev. Mod. Phys. **38**, 1 (1966).
[57] J. A. Hornbeck and J. P. Molnar, Phys. Rev. **84**, 621 (1951); M. P. Teter, F. E. Niles, and W. W. Robertson, J. Chem. Phys. **44**, 3018 (1966).
[58] M. Grössl, M. Langenwalter, H. Helm, and T. D. Märk, J. Chem. Phys. **74**, 1728 (1981); K. Stephan, A. Stamatović, and T. D. Märk, Phys. Rev. A **28**, 3105 (1983).
[59] H. Sugawara, H. Tagashira, and Y. Sakai, J. Phys. D **29**, 1168 (1996).